JOURNAL OF GEOPHYSICAL RESEARCH, VOL. 114, D07301, doi:10.1029/2008JD010990, 2009

Regional variation of the dimethyl sulfide oxidation mechanism in the summertime marine boundary layer in the Gulf of Maine

Hans D. Osthoff,[1,2,3] Timothy S. Bates,[4] James E. Johnson,[4,5] William C. Kuster,[1] Paul Goldan,[1,2] Roberto Sommariva,[1,2] Eric J. Williams,[1,2] Brian M. Lerner,[1,2] Carsten Warneke,[1,2] Joost A. de Gouw,[1,2] Anders Pettersson,[1,2] Tahllee Baynard,[1,2] James F. Meagher,[1] Frederick C. Fehsenfeld,[1,2] A. R. Ravishankara,[1,2,6] and Steven S. Brown[1]

Received 15 August 2008; revised 19 December 2008; accepted 30 December 2008; published 2 April 2009.

[1] Mixing ratios of dimethyl sulfide (DMS) and its nighttime oxidant, the nitrate radical (NO_3), were measured in the summertime marine boundary layer (MBL) of the Gulf of Maine during the New England Air Quality Study–International Transport and Chemical Transformation campaign in 2004. DMS fluxes from the ocean were derived from simultaneous measurements of the wind speed and DMS in seawater. Day and night DMS oxidation rates were determined from modeled OH and measured NO_3 concentrations. The average DMS lifetime with respect to oxidation by OH at noon was 13.5 ± 3.4 (1σ) h, while at night, DMS lifetimes with respect to NO_3 oxidation varied by sampling region from 11 min to 28 h. Oxidation by photochemically generated halogen species likely also played a role during the day, although the nature and extent of the halogen species is more difficult to predict due to lack of halogen measurements. Closure of the DMS budget in the MBL required a vertical entrainment velocity of ~0.4 cm s^{-1}. This study suggests that entrainment of DMS out of the MBL competes with daytime oxidation and that the presence of pollution in the form of NO_x and O_3 in near-coastal regions at night results in nearly complete DMS oxidation within the MBL via reaction with NO_3, with a much smaller contribution from entrainment. One potential implication of near-complete DMS oxidation within the MBL is a reduction of the amount of sulfur available for aerosol formation and growth at higher altitudes in the atmosphere.

Citation: Osthoff, H. D., et al. (2009), Regional variation of the dimethyl sulfide oxidation mechanism in the summertime marine boundary layer in the Gulf of Maine, *J. Geophys. Res.*, *114*, D07301, doi:10.1029/2008JD010990.

1. Introduction

[2] Oceanic emission of dimethyl sulfide (CH_3SCH_3, DMS) is the largest natural source of sulfur in the atmosphere and thus impacts the global budgets of sulfur and aerosols and, therefore, climate [*Charlson et al.*, 1987]. Oxidation of DMS proceeds mainly by the reaction with the hydroxyl radical (OH) by either hydrogen abstraction or addition pathways [e.g., *Hynes et al.*, 1986]:

$$\text{(R1a)} \qquad OH + (CH_3)_2S \rightarrow H_2O + CH_3SCH_2,$$

$$\text{(R1b)} \qquad CH_3SCH_2 \xrightarrow{O_2} CH_3SCH_2O_2,$$

$$\text{(R1c)} \qquad CH_3SCH_2O_2 \rightarrow \text{products},$$

$$\text{(R1d)} \qquad OH + (CH_3)_2S \rightarrow (CH_3)_2SOH,$$

$$\text{(R1e)} \qquad (CH_3)_2SOH \xrightarrow{O_2} \text{products}.$$

In the case of the polluted marine boundary layer (MBL), DMS is also oxidized (via hydrogen abstraction) by the nitrate radical (NO_3) [e.g., *Winer et al.*, 1984]. This oxidant

[1]Chemical Sciences Division, Earth System Research Laboratory, NOAA, Boulder, Colorado, USA.
[2]Also at Cooperative Institute for Research in Environmental Sciences, University of Colorado, Boulder, Colorado, USA.
[3]Now at Department of Chemistry, University of Calgary, Calgary, Alberta, Canada.
[4]Pacific Marine Environment Laboratory, NOAA, Seattle, Washington, USA.
[5]Also at Joint Institute for the Study of the Atmosphere and Ocean, University of Washington, Seattle, Washington, USA.
[6]Also at Department of Chemistry and Biochemistry, University of Colorado, Boulder, Colorado, USA.

0148-0227/09/2008JD010990$09.00

Table 1. Dimethyl Sulfide Reaction Rate Coefficients[a]

Oxidant	k (298 K) (cm^3 $molecule^{-1}$ s^{-1})	k_i/k_{OH}
OH	4.9×10^{-12}	1
NO_3	1.0×10^{-12}	0.2
Cl	1.6×10^{-10}	33
Br	3.0×10^{-14}	0.006
BrO	3.4×10^{-13}	0.07
ClO	6.6×10^{-15}	0.0013
IO	1.2×10^{-14}	0.002
HO_2	$<5 \times 10^{-15}$	<0.001

[a]From *Sander et al.* [2006]. The right column compares individual rate coefficients, k_i, to coefficients for OH.

is produced in the reaction of NO_2 with O_3 and is generally present in large concentrations only at night because of its efficient photolysis and reaction with NO [*Wayne et al.*, 1991]:

$$\text{(R2)} \qquad NO_2 + O_3 \rightarrow NO_3 + O_2,$$

$$\text{(R3a)} \qquad NO_3 + (CH_3)_2S \rightarrow HNO_3 + CH_3SCH_2,$$

reaction (R1b), and

$$\text{(R3b)} \qquad CH_3SCH_2O_2 \rightarrow \text{products}.$$

There is also evidence for daytime removal of DMS other than via reaction with OH. Modeling [e.g., *von Glasow and Crutzen*, 2004] and experimental [e.g., *Saiz-Lopez et al.*, 2006; *Suhre et al.*, 1995; *Wingenter et al.*, 2005; *Yvon et al.*, 1996] studies have implicated the chlorine radical (Cl) and bromine monoxide (BrO) as additional daytime DMS oxidants. Oxidation by other photochemically produced halogen species (e.g., IO [*Allan et al.*, 2000]) (Table 1) and heterogeneous reactions (e.g., with O_3 [*da Rosa et al.*, 2003; *Gershenzon et al.*, 2001]) may also serve as DMS sinks. By contrast, at night there is no competition among oxidants for DMS since NO_3 reaction is the only known gas phase oxidative process in the dark.

[3] Stable sulfur containing products from atmospheric oxidation of DMS include sulfur dioxide (SO_2), methanesulfonic acid (CH_3SO_3H, MSA), and sulfuric acid (H_2SO_4) produced from the subsequent oxidation of SO_2. Methanesulfonic and sulfuric acid have a strong tendency to condense on (and alter) existing aerosols; production of sulfuric acid may also lead to nucleation of new aerosol particles. The DMS oxidation product distribution is dependent on a number of factors, including whether the oxidation is initiated by an addition (e.g., OH, ~25% at 298 K and 1 atm) or an H-abstraction pathway (e.g., NO_3, ~100%, and OH, ~75%) [e.g., *Jensen et al.*, 1992; *Turnipseed et al.*, 1996] and the availability of NO for reaction with peroxy radicals produced in the initial step. The addition pathways lead to products such as dimethylsulfoxide (DMSO) and MSA, and the abstraction leads mainly to SO_2 and ultimately H_2SO_4 [e.g., *Barnes et al.*, 2006]. Because the nocturnal, NO_3-driven DMS oxidation proceeds by abstraction, and because reactions of the resulting peroxy radicals (e.g., the methylthiomethyl (MTM) peroxyl radical, $H_3CSCH_2O_2$) occur in the absence of NO (typically not present at night, except in close proximity to NO_x sources), the DMS oxidation product distribution can be altered by anthropogenic pollution containing NO_x and O_3, which react to produce NO_3. Such alterations may affect the yield of non sea salt (nss) sulfate from DMS oxidation. This in turn can influence aerosol growth and nucleation rates, not only in the MBL but also in the lower and upper troposphere [e.g., *Lucas and Prinn*, 2003]. Thus, the nature and extent of DMS oxidation in the MBL are important parameters in assessing the impact of DMS on global climate.

[4] In this paper, we present simultaneous measurements of NO_3, DMS, DMS fluxes from the ocean surface determined from seawater DMS measurements, and modeled OH mixing ratios in the summertime MBL in the Gulf of Maine. Data were collected during the New England Air Quality Study–International Transport and Chemical Transformation (NEAQS-ITCT) 2004 on the NOAA research vessel Ronald H. Brown (R/V *Brown*) [*Fehsenfeld et al.*, 2006]. The observed DMS mixing ratios were compared to a box model that included DMS emission flux and loss to oxidation, with vertical entrainment as an adjustable parameter. The analysis shows that NO_3 efficiently oxidized DMS at night under conditions of outflow of continental pollution and less efficiently in cleaner, marine air. During the day, DMS removal rates were generally larger than could be accounted for by OH reaction, indicating additional loss pathways, such as vertical entrainment or reaction with halogens. The presence of NO_3 at night significantly affected the fraction of DMS emissions oxidized within the MBL and may therefore also have affected the transport of DMS and condensable sulfur products to higher levels of the atmosphere. Because NO_3 derives principally from anthropogenic NO_x and O_3 pollution, these effects represent an anthropogenic perturbation of the marine sulfur cycle.

2. Field Measurements and Calculations

[5] The 2004 campaign took place during July and August and followed an earlier study, the New England Air Quality Study (NEAQS) 2002, in the region. Results from the earlier study pertinent to DMS oxidation have been reported elsewhere [*Aldener et al.*, 2006; *Stark et al.*, 2007; *Warneke et al.*, 2004]. The 2004 study differed in several aspects: First, NEAQS-ITCT 2004 covered a larger geographical area than NEAQS 2002, which allowed analysis of DMS budgets over a wider range of DMS fluxes and mixing ratios, NO_x and O_3 pollution levels and distance from coastal sources of anthropogenic emissions. Second, the availability of seawater DMS measurements, from which DMS fluxes were calculated for the 2004 study, allowed for a more comprehensive accounting of the DMS budget, particularly with respect to the competition between oxidation and vertical transport.

[6] Measurements of DMS (by gas chromatography–mass spectrometry, GC-MS) and NO_3 (by cavity ring-down spectroscopy, CaRDS) on R/V *Brown* during NEAQS-ITCT 2004 have been described elsewhere [*Goldan et al.*, 2004; *Osthoff et al.*, 2006]. Daytime NO_3 mixing ratios were below the detection limit and were calculated using steady state as described by *Brown et al.* [2005] and *Osthoff et al.*

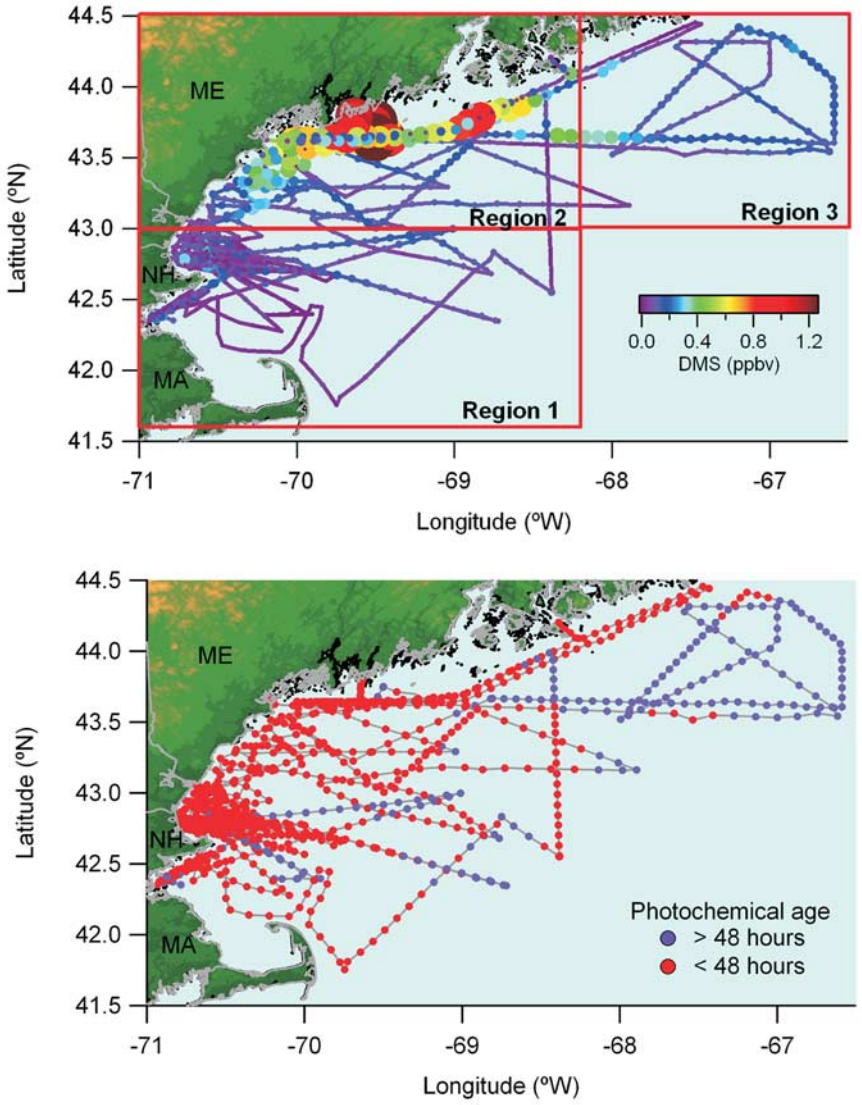

Figure 1. (top) Map of the study area, showing the track of R/V *Brown* during New England Air Quality Study–International Transport and Chemical Transformation (NEAQS-ITCT) 2004, color- and size-coded by dimethyl sulfide (DMS) mixing ratios. The study area was divided into three regions: Region 1 is close to the Massachusetts/New Hampshire coasts and was most affected by continental outflow; region 2 is close to the Maine coast, where the highest DMS mixing ratios (and fluxes) were observed; region 3 is in the northeastern corner of the Gulf of Maine and was furthest removed from continental outflow. (bottom) Track of R/V *Brown*, color-coded by photochemical age, calculated from the ratio of benzene to toluene (see text). Blue points represent a photochemical age >48 h; red data points represent a photochemical age <48 h.

[2006]. Emission rates of DMS from the ocean surface were calculated from measured DMS concentrations in seawater [*Bates et al.*, 1998; *Bates et al.*, 2000] (at 30 min time resolution) and wind speed using the Nightingale parameterization [*Nightingale et al.*, 2000]. Mixing ratios of the hydroxyl radical (OH) were calculated using an explicit chemical model [*Sommariva et al.*, 2008] based on the Master Chemical Mechanism [*Jenkin et al.*, 2003; *Saunders et al.*, 2003]. Measurements of O_3, NO and NO_2 were made by NO-O_3 chemiluminescence. All data were averaged to the time resolution of the GC-MS, which had a 5 min sampling time and produced one data point every 30 min. Gas- and aerosol-phase measurements were made at sampling heights of 15–18 m above the ocean surface.

3. Results

[7] Figure 1 (top) shows an overview of the study area, which was arbitrarily divided into three regions to facilitate the analysis and discussion below. Region 1 was close to the densely populated Massachusetts/New Hampshire coastlines and was most affected by continental outflow of pollutants. Region 2 covered the area along the Maine coast, which was less impacted by anthropogenic pollution

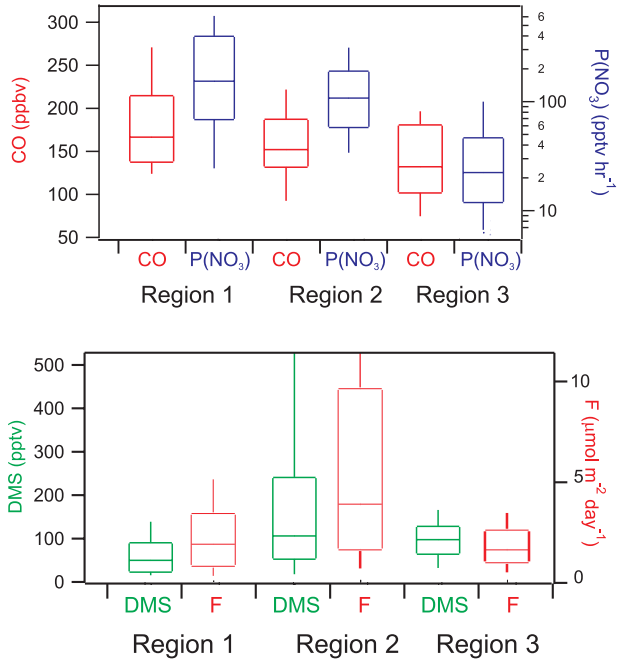

Figure 2. Characterization of the three regions by (top) pollution and (bottom) DMS. Figure 2 (top) shows box-and-whisker plots of CO mixing ratios and the production rate of NO_3, $P(NO_3) = k_2[NO_2][O_3]$, calculated using $k_2 = 1.2 \times 10^{-13}$ $e^{-2450/T}$ cm^3 $molecule^{-1}$ s^{-1} [*Sander et al.*, 2006]. The boxes encompass the 25th, median (50th), and 75th percentiles, and the whiskers the 10th and 90th percentiles, in each region. Region 1 showed the highest, region 2 intermediate, and region 3 the lowest pollution levels. The production rate of NO_3 was more attenuated than the CO mixing ratio. Figure 2 (bottom) shows box-and-whisker plots of DMS mixing ratios and fluxes from the ocean surface. The highest levels of DMS relative to the input from the ocean were seen in region 3.

than region 1. Region 3 was furthest from continental pollution sources. The air masses encountered in region 3 were photochemically older than those in the other regions (by about 1 day), as judged from the toluene to benzene ratio [*Warneke et al.*, 2007]. In all regions, gas-phase DMS was observed, and positive fluxes from the ocean surface were calculated (Figure 2; Table 2). Large variations in observed DMS levels were due to periodic sampling of "hot spots," i.e., areas with large seawater concentrations (see below).

[8] Although these divisions along latitude and longitude boundaries did not achieve complete separation into different chemical regimes, the three regions exhibited distinct levels of DMS emissions and/or anthropogenic pollution as measured, for example, by CO mixing ratios, NO_3 production rates, and photochemical age (Figure 2; Table 2). Comparisons between them therefore illustrate combinations of several effects, including variation in DMS emissions, NO_3 production rates, and nighttime DMS oxidation rates with air mass age. To illustrate the latter effect and to corroborate the results obtained using a geographical sorting, data were also binned by photochemical age into two groups, one younger, and one older, than 48 h (results shown in section 3.4).

3.1. Oxidation of Dimethyl Sulfide (DMS) by NO_3 and OH

[9] Figure 3 shows one example of the diurnal cycle in DMS oxidation rate from data collected over a 24-h period from 21–22 July 2004, during which R/V *Brown* sampled outflow of continental air in region 1. Here, anthropogenic pollution containing NO_2 and enhanced O_3 led to a production rate of NO_3, $P(NO_3)_{avg} = 4.9 \times 10^6$ molecules cm^{-3} s^{-1} (0.7 parts per billion by volume (ppbv) hr^{-1}):

$$P(NO_3) = k_2[NO_2][O_3],$$
$$k_2(298\,K) = 3.2 \times 10^{-17}\,cm^3\,molecule^{-1}\,s^{-1}. \quad (1)$$

Figure 3a shows the mixing ratios of the oxidants NO_3 (measured) and OH (calculated). The time series of DMS mixing ratios in Figure 3b shows an anticorrelation with the oxidant levels in Figure 3a; that is, maxima in the oxidants' mixing ratios correspond to minima in the DMS mixing ratios. Figure 3c shows the DMS flux calculated from seawater DMS concentration and wind speed. Figure 3d shows first-order rate coefficients for chemical loss of DMS, i.e.,

$$k'_{NO_3} = k_{NO_3+DMS}[NO_3] \quad (2)$$

$$k'_{OH} = k_{OH+DMS}[OH], \quad (3)$$

Table 2. Average, Median, and Standard Deviation of O_3, NO_2, OH, CO, and Dimethyl Sulfide Mixing Ratios as Well as Dimethyl Sulfide Fluxes in the Three Regions of the Study Area[a]

Average (Median) ± 1σ	Region 1	Region 2	Region 3
NO_2 (ppbv)	3.0 (1.6) ± 3.4	1.8 (1.2) ± 1.9	0.4 (0.2) ± 0.6
O_3 (ppbv)	42 (37) ± 16	42 (37) ± 19	47 (48) ± 12
OH at noon (pptv)	0.26 (0.27) ± 0.02	0.25 (0.27) ± 0.03	0.22 (0.22) ± 0.04
CO (ppbv)	183 (166) ± 65	159 (152) ± 50	137 (131) ± 44
NO_y (ppbv)	5.3 (3.2) ± 5.6	4.2 (3.3) ± 3.7	1.7 (1.1) ± 2.3
$P(NO_3)$ (ppbv hr^{-1})	0.27 (0.15) ± 0.31	0.17 (0.11) ± 0.21	0.04 (0.02) ± 0.06
Photochemical age (h)	33 (31) ± 17	32 (31) ± 11	57 (56) ± 16
DMS (pptv)	65 (50) ± 58	197 (106) ± 229	100 (57) ± 57
DMS flux (μmol m^{-2} d^{-1})	2.5 (1.9) ± 2.3	7.9 (3.9) ± 10.7	1.9 (1.6) ± 1.2

[a]The production rate of NO_3, $P(NO_3) = k_2[NO_2][O_3]$, was calculated using $k_2 = 1.2 \times 10^{-13}$ $e^{-2450/T}$ cm^3 $molecule^{-1}$ s^{-1} [*Sander et al.*, 2006]. The photochemical age was calculated using the toluene to benzene ratio [*Jobson et al.*, 1998; *Roberts et al.*, 1984] and an emission factor of 3.7 [*de Gouw et al.*, 2005].

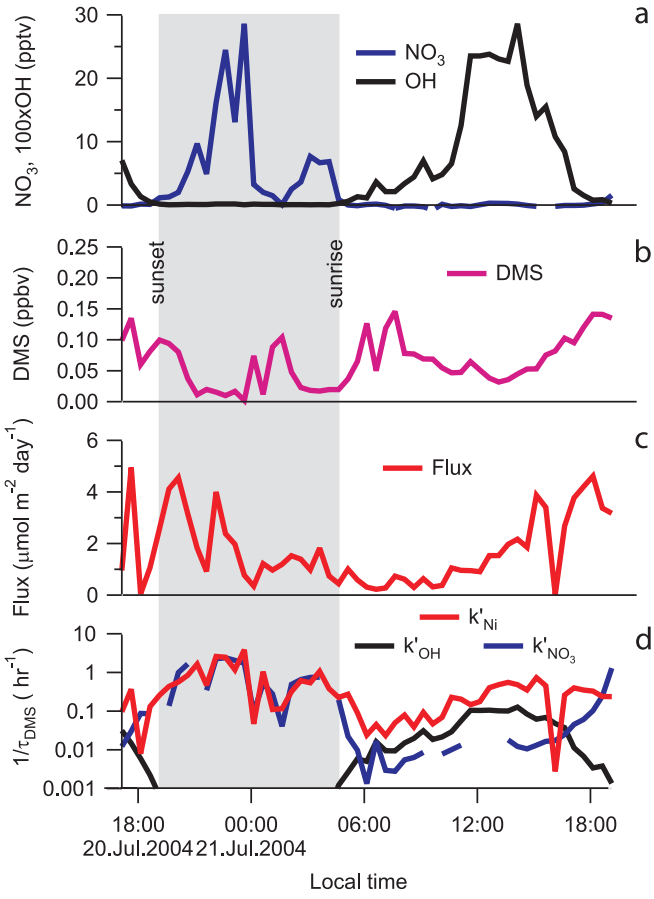

Figure 3. Example 24-h period from 21–22 July 2004. On this day, R/V *Brown* sampled continental outflow off the New Hampshire coast (region 1). (a) Abundances of the oxidants NO_3 (measured) and OH (calculated). (b) DMS mixing ratios. (c) Surface fluxes, calculated using the parameterization by *Nightingale et al.* [2000]. (d) Inverse steady state lifetimes for DMS ($1/\tau_{DMS}$), calculated using equation (4). First-order loss rate coefficients for loss of DMS to NO_3 (k'_{NO_3}, equation (2)) and OH (k'_{OH}, equation (3)) are superimposed. In this example, the rate coefficient for nocturnal oxidation by NO_3 was equal to the inverse steady state DMS lifetime, indicating DMS budget closure with respect to oxidation and the absence of vertical entrainment and other loss pathways.

and inverse steady state DMS lifetimes, $1/\tau_{DMS}$. At steady state, the DMS lifetime is given by

$$\tau_{DMS} = \frac{h_{MBL}}{F}[DMS]. \quad (4)$$

Here, F is the DMS flux from the ocean surface, and h_{MBL} is the height of the MBL. The latter did not exhibit a diel profile and was constant at about 100 m [*Angevine et al.*, 2006]. Equation (4) is valid for the case of an MBL that is well mixed with respect to DMS and its oxidants.

[10] The induction time required for approach to steady state is approximately four to five times the inverse of the first-order loss rate coefficient [*Pilling and Seakins*, 1995]. In this example, the DMS lifetime with respect to NO_3 oxidation at night, $1/k'_{NO_3}$, was ~0.5 h and with respect to OH oxidation during the day, $1/k'_{OH}$, ~10 h. As a result, DMS likely achieved a steady state at night but not during the day. In this example, losses via oxidation by NO_3 at night were approximately equal to the steady state DMS lifetime (calculated from observed mixing ratios and the input from the ocean surface), implying that the nocturnal lifetime of DMS was controlled entirely by NO_3 and that other DMS losses, e.g., venting out of the marine boundary layer, were small. During the day (both in this example and in general for this data set), the first-order loss rate coefficient to OH was at least one order (often several orders) of magnitude less than the inverse DMS steady state lifetime; that is, the OH oxidation rate was too slow to bring DMS into a steady state during daytime. This result and the modeling analysis presented in section 3.3 below are consistent with other active daytime DMS loss processes (e.g., entrainment, oxidation by halogens, or heterogeneous reactions).

[11] Shown in Figure 4 are plots of observed DMS mixing ratios against NO_3 (nighttime data only) and OH (daytime data only) mixing ratios for the entire campaign, color coded by region. Nighttime mixing ratios of DMS and NO_3 were strongly anticorrelated; this anticorrelation was a persistent feature of the entire data set. In contrast, the daytime mixing ratios of DMS were only weakly anticorrelated with the calculated OH (Figure 4, right). In region 1, $P(NO_3)$ was largest, and NO_3 regulated DMS at night. Similar to the result shown in Figure 3, the observed DMS levels were in balance between oceanic emissions and oxidation by NO_3. In the other regions, NO_3 production rates and mixing ratios were smaller. In region 2, NO_3 mixing ratios were suppressed in spite of a production rate of 1.4×10^6 molecules cm^{-3} s^{-1} (0.2 ppbv hr^{-1}) (Table 2), in part because the emission rate of DMS from the ocean and DMS mixing ratios were large. In region 3, NO_3 mixing ratios were small due to both low production (60 pptv hr^{-1}) caused by low NO_2 mixing ratios (median 0.2 ppbv; Table 2) and other efficient sinks (e.g., fog [*Osthoff et al.*, 2006]). The mixing ratios of OH were much less dependent on the overall level of pollution and similar in all regions (Table 2; Figures 4 and 5). In contrast, NO_3 was spatially inhomogeneous; as a result, nocturnal lifetimes of DMS varied considerably across the different regions, while daytime oxidation rates were approximately constant.

3.2. Average Diurnal Profiles

[12] The example in Figure 3 clearly shows the effect of oxidant levels on DMS mixing ratios across a single 24 h period. On many other individual days, however, variability in the mixing ratios of NO_3, OH, and DMS fluxes due to changes in air mass and in sampling location effectively masked such diel effects. However, the averages of DMS, NO_3 and OH mixing ratios as a function of time of day within each of the three regions, as shown in Figure 5, did show a clear diurnal pattern that serves to illustrate the regional variation in DMS oxidation chemistry. The DMS input from the ocean surface determined from seawater DMS and wind speed (not shown) did not vary as a function of time of day. In the polluted case (region 1; Figure 5, top), the diurnal profile of DMS had two maxima: the first about 1 h after sunrise and the second at sunset. The DMS

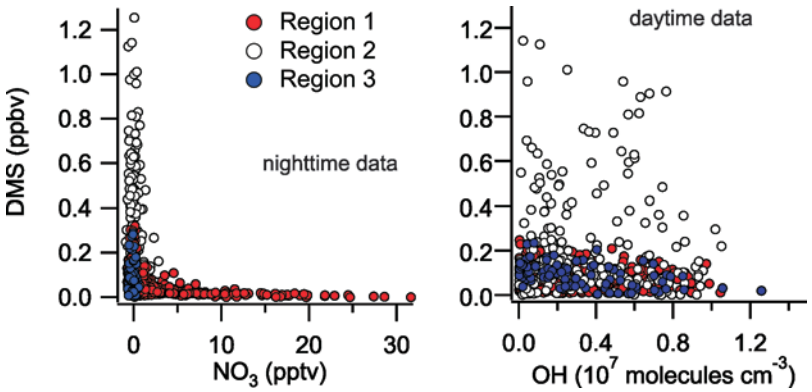

Figure 4. (left) Plots of DMS versus measured NO_3 (nighttime data only, i.e., solar zenith angle > 90°) and (right) calculated OH (daytime data only, i.e., solar zenith angle < 90°). The NO_3-DMS anticorrelation was clearest in the polluted case (region 1) and less obvious in the remote marine area (region 3). The correlation of DMS with OH was considerably weaker than with NO_3 in all regions.

maxima coincided with minima in the mixing ratios of NO_3 and OH (so-called radical gaps [*Brown et al.*, 2004; *Platt et al.*, 2002; *Warneke et al.*, 2004]). The diurnal cycle in the top of Figure 5 corroborates that observed during the NEAQS 2002 campaign [*Stark et al.*, 2007], during which the sampling occurred primarily near the coast, similar to the area sampled in region 1 during the 2004 campaign. Even so, the DMS mixing ratios in region 1 were larger at night in 2004 than during the 2002 campaign (by a factor of 2), consistent with smaller average NO_2 abundance (3.0 ppbv in 2004, 4.5 ppbv in 2002) and reduced relative $P(NO_3)$.

[13] Figure 5 (middle) shows the average diurnal pattern of DMS, NO_3, and OH in region 2, where large DMS fluxes from the ocean surface were observed (Table 2). On average, the NO_3 mixing ratios were much lower in region 2 than in region 1, and the diurnal cycle of DMS did not show a measurable time-of-day dependence. In this region, the DMS flux from the ocean exceeded the capacity of the oxidants (including halogens) within the MBL to completely remove the emitted DMS, suggesting that entrainment to the lower troposphere contributed to the budget of DMS within the MBL (see below).

[14] Figure 5 (bottom) shows diurnal cycles of the mixing ratios of DMS and its oxidants in the Eastern part of the Gulf of Maine (region 3), which was less influenced by anthropogenic pollution. The averages in this region contain data from only 2 days of sampling and are thus more prone to variability than the other regions. The average shown in Figure 5 (bottom) is treated here as representative for this region. Average DMS mixing ratios were higher at night than during the day. The observed decrease during the day is consistent with photochemical oxidation by OH, while the increase after sunset is consistent with reduced nighttime oxidation by NO_3 compared to other regions. The reduced contribution of NO_3 is consistent with a small average $P(NO_3)$ (4.0×10^{-5} molecules cm^{-3} s^{-1}, 58 pptv hr^{-1}; Table 2), but also with competition between different sinks for the available NO_3. For example, the prevalence of fog in this region (affecting ~40% of the data) likely led to a large increase in the heterogeneous uptake rates of N_2O_5 and NO_3 [*Osthoff et al.*, 2006], such that only a fraction of the already slow NO_3 production in this region was actually available as an oxidant for DMS.

[15] The time-of-day dependence of the first-order chemical DMS loss rate coefficients (k'_{NO_3} and k'_{OH}) is shown in Figure 6, sorted by region. Nighttime oxidation by NO_3 showed a clear regional dependence, driven by anthropogenic pollution as discussed above; in contrast, daytime k'_{OH} was not strongly dependent on sampling region. Although low levels of nighttime OH were predicted by the MCM simulation, the contribution of nocturnal oxidation of DMS by OH was negligible (<1%) in all regions; by contrast, the daytime contribution of NO_3 to DMS oxidation was small but sometimes considerable (up to 40%), consistent with our previous analysis of oxidation rates of a variety of VOCs due to daytime NO_3 production [*Osthoff et al.*, 2006]. In the current analysis, where we have calculated this contribution in an average sense across regions, the oxidation of DMS via NO_3 in the daytime in region 1 was predicted to be 7% of the total DMS oxidation rate via NO_3 and OH (excluding halogens). The contribution of NO_3 to daytime DMS oxidation was considerably lower in region 3 than in the other two, more polluted regions, but is not representative of remote marine regions, where the NO_3 production rate from equation (1) would be on the order of 1 pptv hr^{-1} (i.e., 30 ppbv O_3, 10 pptv NO_2).

3.3. Modeling DMS in the Marine Boundary Layer (MBL)

[16] A simple model was used to simulate the average diurnal profiles of DMS mixing ratios observed in the three regions. This model assumes a MBL of 100 m depth (h_{MBL}), on the basis of rawinsondes, which showed the persistence of a shallow, stable MBL in this region during the study period. Eddy turnover times in this layer were on the order of 20–30 min [*Angevine et al.*, 2006]. The model integrates equation (5), which includes chemical losses to OH and NO_3, flux from the ocean surface, and vertical entrainment out of the marine boundary layer:

$$\frac{d}{dt}[\mathrm{DMS}] = \frac{F}{h_{\mathrm{MBL}}} - \left(\frac{v_E}{h_{\mathrm{MBL}}} + k'(\mathrm{ODH}) + k'(\mathrm{NO_3})\right) \times [\mathrm{DMS}] \quad (5)$$

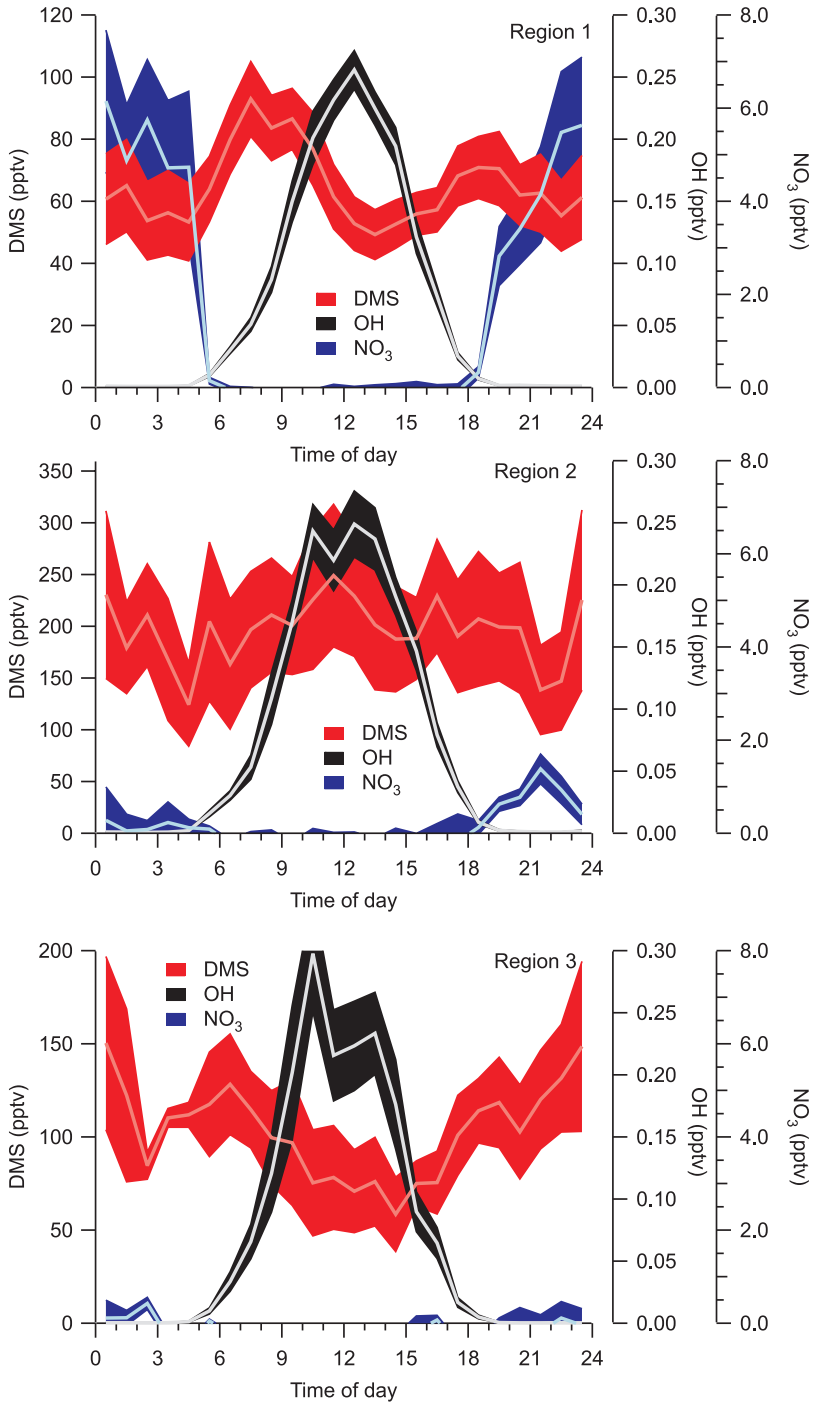

Figure 5. Diurnal averages of NO_3, DMS, and OH. The shading shows $\pm 1\sigma$ of the measurements. In region 1, close to the coast, mixing ratios of DMS peaked during dawn and dusk, during periods of smallest radical production. In region 2, there was no obvious diurnal pattern, consistent with DMS mixing ratios being controlled by surface emissions, which did not show a time-of-day dependence. In the remote case, DMS mixing ratios decreased during the day, consistent with oxidation by OH, and increased at night due to reduced NO_3 production and mixing ratios.

Here v_E is the vertical escape (entrainment) velocity, and $k'(OH)$ and $k'(NO_3)$ are as defined in equations (2) and (3). Horizontal transport is neglected because it is assumed unimportant in the diurnally average data to which the model is compared. To minimize artifacts from outliers in the data, median [OH], [NO_3], F, and [DMS] values (as functions of time of day) were used as model inputs. A spin-up time of 1 day ensured that simulations were independent of the initial DMS concentration. The model assumes complete mixing within the 100 m layer thickness nearest the surface. This assumption is approximately correct in the limit where the chemical transformation is slower than the time scale of

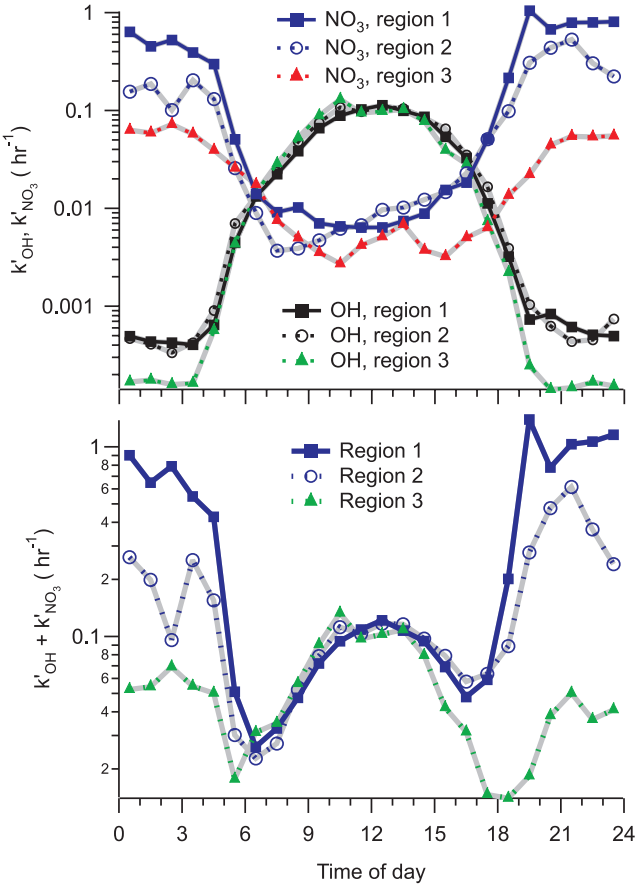

Figure 6. (top) Diurnal averages of first-order DMS loss rate coefficients for reaction with NO_3 (k'_{NO_3}) and OH (k'_{OH}); k'_{NO_3} was enhanced in region 1, i.e., in the presence of anthropogenic pollution (NO_x and O_3), whereas k_{OH} did not exhibit a regional dependence. (bottom) Sum of the calculated chemical loss rate, $k'_{NO_3} + k'_{OH}$, from Figure 6 (top) showing minimum oxidation rates in early morning and late afternoon.

the mixing. Particularly in region 1, where the average DMS lifetime at night with respect to NO_3 oxidation of 1.7 h approached the 0.3–0.5 h MBL turnover time, there is a potential for development of vertical gradients. If so, the observed surface level concentrations of DMS are larger than the average concentration across the layer. In the absence of vertically resolved data on chemical composition, we have modeled the chemistry within the MBL as though mixing were complete.

[17] Halogen containing radicals, known oxidants of DMS [e.g., *Langner and Rodhe*, 1991], were not measured on R/V *Brown* during NEAQS-ITCT 2004. To simulate the potential contribution of photochemically generated halogen radicals, we arbitrarily used atomic Cl as a proxy for all reactive halogens and constrained its mixing ratios to a fixed ratio of 1:50 relative to OH on the basis of an estimate of Cl atom concentrations derived from halogen measurements on Appledore Island [*Pszenny et al.*, 2007]. This ratio of Cl to OH is similar to the 1:80 ratio inferred by *Stark et al.* [2007]; the use of a larger fraction of Cl in the current work puts a slightly lower (more conservative) limit on the contribution of entrainment.

[18] Although there were cases in which the production and chemical loss rates of DMS were in approximate balance (e.g., Figure 3), it was generally the case that the DMS input was considerably larger than the known chemical sinks ($k'_{NO_3} + k'_{OH}$). Therefore, a nonzero vertical entrainment velocity was needed to bring simulations and observations in agreement. We evaluated entrainment velocities of 0.2, 0.4, and 0.6 cm s^{-1} and found best agreement between model and simulation with the intermediate value of 0.4 cm s^{-1} when oxidation by halogens was included in the model (Figure 7). This entrainment falls within the range of 0.12 to 0.76 cm s^{-1} measured by *Faloona et al.* [2005] in the Eastern Pacific, and is modestly larger than the 0.25 cm s^{-1} assumed by *Stark et al.* [2007] for the NEAQS 2002 study and the 0.168 cm s^{-1} given by *Yvon et al.* [1996] for observations made in the South Pacific.

[19] Simulated and observed diurnal profiles are shown in Figure 7 for each region. In region 1 (Figure 7, top), the observed diurnal profile exhibited a maximum at dusk and one at dawn. The simulation is in somewhat better agreement with the observations if oxidation by halogens is included (dashed curves). The observed morning maximum was larger than the evening, but the model results show the opposite trend between the two. The difference between modeled and measured diurnal profiles may indicate that chemical sinks were underestimated in late day; however, the statistical variation in the dawn and dusk maxima was large, so that relative differences are difficult to interpret. While the sonde data generally showed the mixing height to be invariant [*Angevine et al.*, 2006], it is possible that small variations in boundary layer dynamics may also have played a role in the observed DMS profiles.

[20] In region 2 (Figure 7, middle), the measurements did not exhibit a clear diurnal pattern. In contrast, the simulation predicts DMS maxima after sunrise and before sunset and larger mixing ratios during the day than during the night. As before, the simulation is in somewhat better agreement with the observations if oxidation by halogens is included (dashed curves). However, the day-night contrast in the modeled traces in region 2 are smaller than in region 1, so that the simulation is consistent with the observations since it lies within the statistical variability at all times of day.

[21] In region 3 (Figure 7, bottom), the measured contrast in DMS concentrations between day and night is well reproduced by the simulation (keeping in mind that the vertical offsets are determined by the entrainment velocity and are thus arbitrary). DMS mixing ratios increased at night and decreased during the day, consistent with daytime oxidation of DMS playing a much larger role than its nighttime oxidation. Addition of oxidation by halogens did not noticeably improve the agreement between simulation and experiment, suggesting that oxidation by halogens may have been less important in this case.

3.4. Comparison of Data Sorted by Region With Data Sorted by Photochemical Age

[22] Figure 8 shows simulated and observed diurnal DMS profiles for data that was sorted by photochemical age, on the basis of the toluene to benzene ratio [*Warneke et al.*,

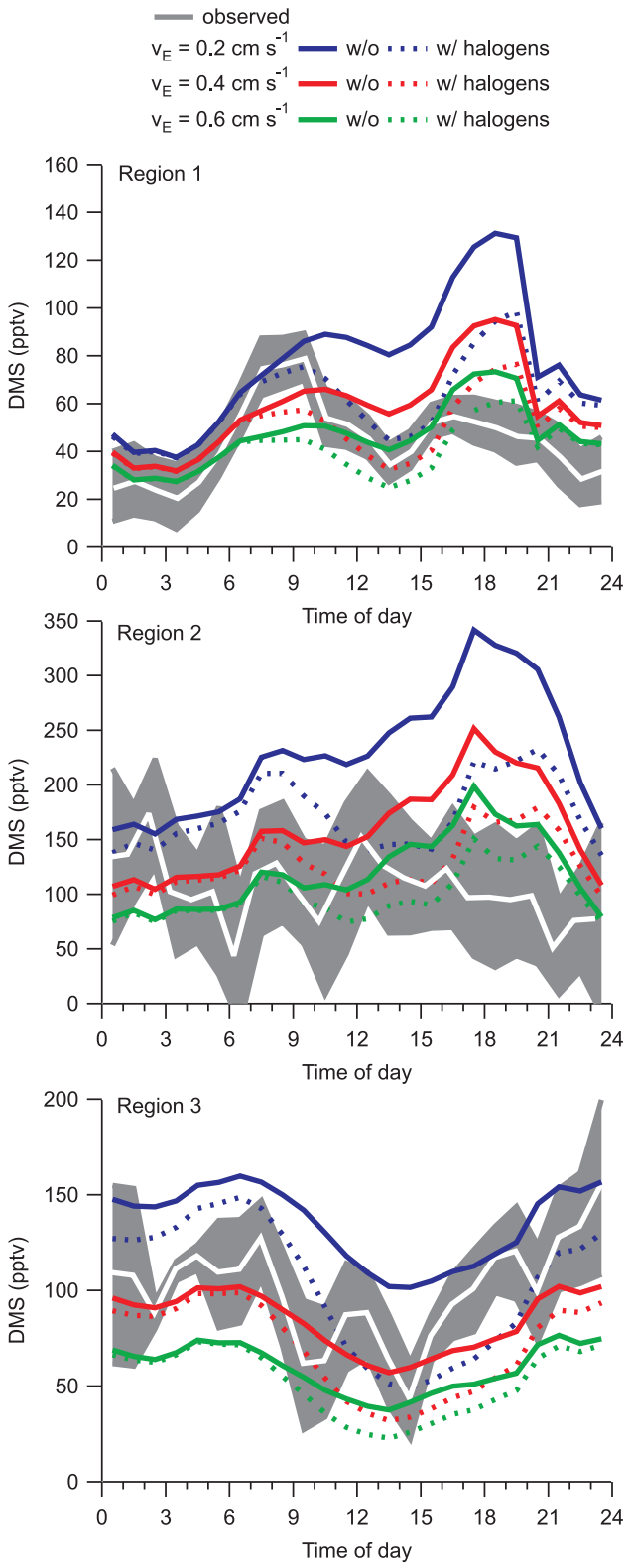

Figure 7. Simulation of the DMS diurnal profile in the three regions. The shaded area represents the observed diurnal profile of DMS (median, $\pm 1\sigma$) with the median shown as a white trace. The simulations include vertical entrainment (v_E = 0.2, 0.4, and 0.6 cm s^{-1}) and chemical losses to NO_3 and OH. The dashed lines include oxidation of DMS by halogen radicals, in this case assumed to be Cl and scaled to OH by a factor of 1:50.

2007], into two bins less than and greater than 48 h. This age was chosen because it roughly sorted the data in half and therefore provided good statistics (the maximum photochemical age observed in this study was 83 h). Furthermore, the ratio of NO_x to NO_y showed an exponential decrease with photochemical age, with a time constant of 1.3 days, such that the choice of division at 2 days separated the data at the point where this ratio was approximately 0.2. For this analysis, data points with very large DMS surface-to-air fluxes (>10 μmol m^{-2} d^{-1}) were excluded. These points can be accounted for in the regional sorting, but appear as outliers in a sorting that is done by photochemical age only. In the younger photochemical age case (Figure 8, top), the observed diurnal profile resembled that in Region 1 (Figure 7, top), with lower DMS mixing ratios at night than during the day. The DMS maxima in the early morning and late afternoon were slightly less pronounced but still clear. The diurnal profile is reproduced by the simulation with the intermediate entrainment velocity of 0.4 cm s^{-1} and halogen oxidation. For the photochemically aged air masses (Figure 8, bottom), DMS mixing ratios were larger at night than during the day. Overall, the results obtained using data sorted by photochemical age are consistent with the results obtained using the regional sort of the data.

[23] The clear change in diurnal pattern across the three regions (and between photochemically young and old air masses), from a nighttime minimum to a nighttime maximum in DMS mixing ratios, follows the trend in NO_3 production rates and illustrates the way in which continental NO_x sources influence DMS oxidation. The comparison of modeled to measured diurnal profiles across the three regions showed the strong influence of NO_x and O_3 pollution on nighttime DMS oxidation in the near source region (region 1), the increased nocturnal DMS lifetime in the aged air masses (region 3), and the roughly comparable day and night levels of DMS in the intermediate region (2). The latter was also influenced by much larger emissions of DMS. Models across all three regions show better agreement with measurements if daytime oxidants in addition to OH, such as halogens, are included. This is broadly consistent with previous studies, although the detailed mechanisms for photochemical generation of halogen containing radicals are uncertain. Further, the model-measurement agreement is best for a vertical entrainment velocity of 0.4 cm s^{-1}. The next section explores the implications of the competition between day and nighttime oxidation and vertical entrainment of DMS.

3.5. Potential Implications for nss-Sulfate and Aerosol Formation Outside the MBL

3.5.1. Mechanistic Considerations

[24] A shift of DMS oxidation from daytime (OH) to nighttime (NO_3) may affect the yields of SO_2, H_2SO_4, and, ultimately, sulfate aerosol due to differences in the DMS oxidation pathways [*Lucas and Prinn*, 2002, 2005a, 2005b; *Stark et al.*, 2007], although these shifts depend critically on the mechanism for DMS oxidation and the reactions that occur after the initial oxidation step, all of which are highly uncertain. One key intermediate is the methylthiomethyl (MTM) peroxyl radical, $CH_3SCH_2O_2$, which is generated subsequent to H-atom abstraction from DMS (reaction (R1b)). Under polluted (i.e., high NO_x) conditions during

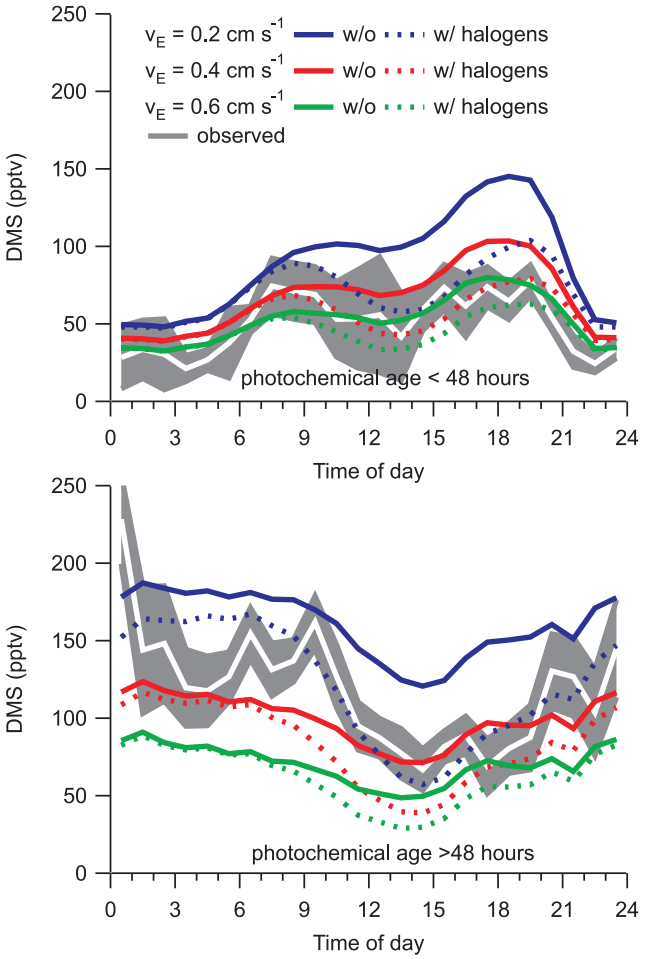

Figure 8. Simulated and observed DMS diurnal profiles for photochemical ages (determined from toluene to benzene ratio) less than and greater than 48 h. Data points with DMS fluxes ≥ 10 μmol m^{-2} d^{-1} were excluded. In the photochemically aged air masses, the DMS diurnal profile exhibits a minimum at midday, consistent with daytime oxidation by OH. In the photochemically young air masses, the DMS mixing ratios are smaller at night than during the day, consistent with increased nocturnal oxidation by NO_3.

the day, this peroxyl radical reacts with NO, and the resulting alkoxy radical most likely decomposes to CH_3S and CH_2O:

(R4) $CH_3SCH_2O_2 + NO \rightarrow CH_3SCH_2O + NO_2$,

(R5) $CH_3SCH_2O \rightarrow CH_3S + CH_2O$,

(R6) $CH_3S + O_2 \rightarrow CH_3SO_2 \rightarrow\rightarrow SO_2$.

At night, there are a number of reactions that the MTM peroxyl radical may undergo. First, it may react with HO_2 to give CH_3SCH_2OOH, a compound that likely undergoes rapid deposition back to the ocean surface, removing the sulfur from the atmosphere [*Singh*, 1995]. Second, it may decompose to CH_3S and CH_2O subsequent to reactions with other peroxy radicals or NO_3 to ultimately give SO_2. It may also react with NO_2 in a reversible equilibrium to yield a peroxy nitrate, although the equilibrium likely favors the reactants rather than the nitrate product [*Barnes et al.*, 2006]:

(R7) $CH_3SCH_2O_2 + HO_2 \rightarrow CH_3SCH_2OOH + O_2$,

(R8) $CH_3SCH_2O_2 + NO_3 \rightarrow CH_3SCH_2O + O_2 + NO_2 \rightarrow\rightarrow SO_2$,

(R9) $CH_3SCH_2O_2 + NO_2 \leftrightarrow CH_3SCH_2O_2NO_2$.

The amount of SO_2 and H_2SO_4 produced from DMS oxidation by NO_3 is uncertain; product studies in smog chambers have found yields in the range of 10% to 68% [*Barnes et al.*, 2006]; the largest SO_2 yields were observed in chamber studies at NO_x concentrations within a range small enough to represent typical ambient levels [*Yin et al.*, 1990]. Although it is difficult to predict the impact of NO_3 driven DMS oxidation in the MBL (see, e.g., the discussion of *Stark et al.* [2007]), nocturnal DMS oxidation clearly has the potential to change the yields of various oxidation products and may ultimately influence the yield of sulfate aerosol.

3.5.2. Potential Impact on Vertical Transport of Sulfur Species

[25] Oxidation of DMS by NO_3 in the polluted MBL may also change the spatial distribution of DMS and its oxidation products (Figure 9). As noted above, the oxidation products of DMS include water-soluble compounds such as SO_2, DMSO, MSA, H_2SO_4, CH_3SCH_2OOH, etc. Many of these compounds are rapidly lost to dry deposition to the ocean surface and to heterogeneous uptake on sea salt aerosol. For example, SO_2, a major product of DMS oxidation, has a lifetime with respect to dry deposition to the ocean surface of 2.5 h in a 100 m deep boundary layer assuming a deposition velocity $\sim$1.2 cm s^{-1} [e.g., *De Bruyn et al.*, 2006]. This deposition lifetime is shorter than its lifetime with respect to photochemical oxidation by OH ($\sim$60 h, assuming [OH] = 5×10^6 molecules cm^{-3}) [*Sander et al.*, 2006]. This example of rapid, calculated SO_2 depositional loss is specific to the shallow boundary layers during this campaign. In contrast, DMS is not lost to dry deposition since the ocean surface is usually supersaturated with respect to DMS, and its rate coefficient for uptake on sea salt aerosol, even when subsequent chemistry such as heterogeneous oxidation by O_3 is taken into account [*da Rosa et al.*, 2003; *Gershenzon et al.*, 2001], is orders of magnitude smaller than the uptake coefficients of the various DMS oxidation products.

[26] Following entrainment of DMS out of the marine boundary layer, oxidation of DMS to SO_2 (and other products) yields H_2SO_4 (the most important product of photochemical SO_2 oxidation) that condenses to form sulfate aerosol and cloud condensation nuclei (CCN). Therefore, the degree to which DMS oxidation takes place within the marine boundary layer, where dry deposition to the ocean surface of its initial oxidation products can compete with further oxidation to H_2SO_4, may affect the

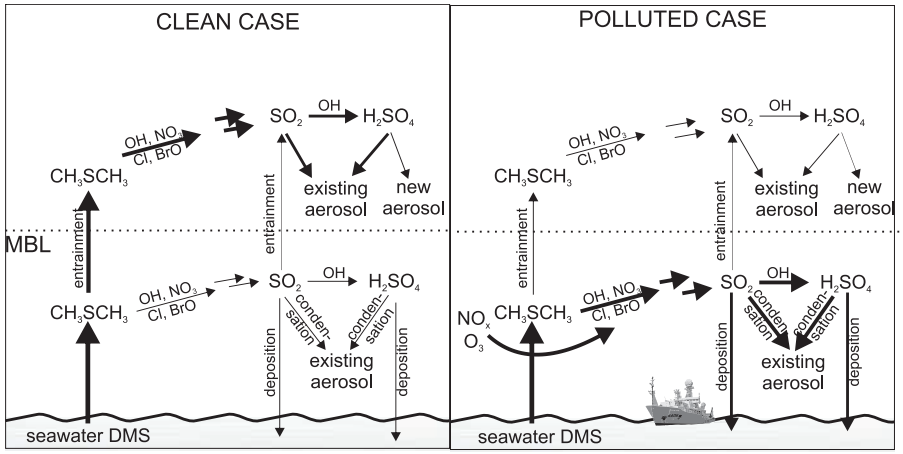

Figure 9. Conceptual illustration of the impact of DMS oxidation in the polluted marine boundary layer (MBL). (left) Unpolluted case. Some of the DMS emitted from the ocean surface is oxidized in the MBL, and the oxidation products (e.g., SO_2, H_2SO_4) condense on the existing aerosol surface or are lost to dry deposition to the ocean surface. The remaining DMS entrains out of the MBL, where its oxidation may act as a source of condensable sulfur in higher layers, depending on the transport dynamics. (right) Polluted case, where outflow of continental pollution in the form of NO_x and O_3 enhances DMS oxidation rates in the MBL, reducing vertical entrainment of sulfur species. The arrow thickness qualitatively represents relative rates for different processes between the two cases.

yield of non–sea salt sulfate aerosol from marine sulfur emissions. The nature and extent of this effect would depend on the atmospheric dynamics above the shallow, 100 m layer used to model these results. Since the coastal environment in which this study took place is known to have the potential for multiple stable layers, surface level observations do not place constraints on the transport of sulfur species above the marine boundary layer. However, increased nocturnal oxidation of DMS within the marine boundary layer in the polluted case is likely to lead to increased loss of the products to dry deposition compared to the unpolluted case.

[27] We used a box model to give a rough estimate of the potential impact of enhanced DMS oxidation by NO_3 in the polluted MBL on the vertical entrainment of sulfur species. Reactions considered in this model are listed in Table 3, and the results are summarized in Table 4. The model assumes a constant DMS flux from the ocean surface of 2.0 μmol m^{-2} d^{-1}, a 100 m deep MBL, absence of dry deposition of DMS, a vertical entrainment velocity of 0.4 cm s^{-1} and constant DMS oxidation rates (Table 3). The model also includes reactive uptake of SO_2 and DMS on sea salt aerosol. For simplicity, the only DMS oxidation product considered was SO_2. The model therefore underestimates the amount of sulfur lost in the MBL, since other oxidation products such as H_2SO_4 likely undergo more rapid deposition than does SO_2. Vertical entrainment of sea salt aerosol (and sulfur species deposited on it) was assumed to be negligible.

[28] The model was run for four scenarios: OH-initiated oxidation (midday), NO_3-initiated oxidation in the "polluted" case (region 1), NO_3-initiated oxidation in the "clean" marine case (region 3), and NO_3-initiated oxidation in an

Table 3. Mechanism and Parameters Used in the Calculation Described in Section 3.5[a]

Reaction	Parameter	Value
$OH_{(g,MBL)} + DMS_{(g,MBL)} \rightarrow SO_2$ (midday)	$k'_{OH} = k_{OH+DMS}$ [OH]	3×10^{-5} s^{-1} (this work)
	yield of SO_2(g)	75 ± 5% [*Barnes et al.*, 2006]
$NO_{3(g,MBL)} + DMS_{(g,MBL)} \rightarrow$ products SO_2 (night)	$k'_{NO_3} = k_{NO_3}$+DMS [NO_3]	region 1: 3×10^{-4} s^{-1} (this work); region 3: 1×10^{-5} s^{-1} (this work); remote MBL: 2.5×10^{-6} s^{-1}
	yield of SO_2(g)	62 ± 7% [*Yin et al.*, 1990]
$DMS_{(aq,ocean)} \rightarrow DMS_{(g,MBL)}$	F(DMS)	2.0 μmol m^{-2} d^{-1} (this work)
$DMS_{(g,MBL)} \rightarrow DMS_{(aq,aerosol)}$	k_{het}(DMS)	1×10^{-6} s^{-1} [*Gershenzon et al.*, 2001]
$SO_{2(g,MBL)} \rightarrow SO_{2(aq,ocean)}$	$v_d(SO_2)$	1.2 cm s^{-1} [*De Bruyn et al.*, 1998]
	$k_d(SO_2)$	1.2×10^{-4} s^{-1}
$SO_{2(g,MBL)} \rightarrow SO_{2(aq,aerosol)}$	$k_{het}(SO_2)$	$\leq 1.4 \times 10^{-3}$ s^{-1}
$SO_{2(g,MBL)} \rightarrow SO_{2(g,trop)}$	$v_E(SO_2)$	0.4 cm s^{-1} (this work)
	$k_E(SO_2)$	4.0×10^{-5} s^{-1}
$DMS_{(g,MBL)} \rightarrow DMS_{(g,trop)}$	v_E(DMS)	0.4 cm s^{-1} (this work)
	k_E(DMS)	4.0×10^{-5} s^{-1}

[a]The rates of heterogeneous uptake of SO_2 were calculated using $k_{het} = 1/4 \times c \times \gamma \times S_{aerosol}$, with $S_{aerosol}$ = surface area density = 200 μm^2 cm^{-3}, c = mean molecular speed of SO_2 = 314 m/s, and uptake probability γ ($\leq$0.09 [*Gebel et al.*, 2000]). Remote marine boundary layer values were calculated with an assumed [NO_3] of 0.1 pptv.

Table 4. Results of the Box Model Calculations Described in Section 3.5[a]

	[DMS] at Steady State (pptv)	[SO_2] at Steady State (pptv)	Fraction of Sulfur Entrained in the Form of DMS (%)	Fraction of DMS Converted to SO_2 in MBL (%)	Fraction of Sulfur Entrained in the Form of SO_2 (%)	Fraction of Sulfur Lost to Dry Deposition (%)
OH (midday)	79	1.1	57	31	0.8	30
NO_3 (night, "polluted," region 1)	16	1.8	12	54	1.3	53
NO_3 (night, "aged," region 3)	109	0.6	78	13	0.4	12
NO_3 (night, "remote MBL")	130	0.1	94	4	0.1	4

[a]Abbreviations are as follows: DMS, dimethyl sulfide; MBL, marine boundary layer.

estimate of a "remote" marine case [e.g., *Bandy et al.*, 1996]. The model runs were initialized with DMS and SO_2 mixing ratios at steady state (Table 4). Mixing ratios of SO_2 were calculated to be small, consistent with its rapid deposition. During the day, 57% of the sulfur emitted from the ocean surface vented out of the MBL, while 30% was lost to deposition. For nighttime conditions of the scenarios based on observations, the amount of sulfur vented ranged from 78% (region 3, cleanest observed in this study) to 12% (region 1, polluted), with 12–53% of the sulfur emitted from the ocean was lost to deposition. For the assumed remote marine case, we estimate that 94% of the DMS is entrained at night, and only 4% of the sulfur is lost to dry deposition.

4. Conclusions

[29] The abundance of the nitrate radical, and consequently, the nocturnal oxidation rate of DMS within the MBL differ regionally because both scale with NO_x and O_3 from anthropogenic sources (e.g., emissions from shipping, continental outflow). For example, DMS was oxidized more rapidly at night in outflow of anthropogenic pollution in the near coastal region, but not in the more remote region, where NO_x levels were considerably lower and the impact of NO_3 on DMS oxidation was smaller. A second conclusion from this study is that oxidation accounted for a larger fraction, and vertical entrainment a smaller fraction of DMS loss from the MBL at night than during the day. The entrainment velocity needed to close the DMS budget ($0.4\ cm^{-1}$) was within the range of current literature values [*Faloona et al.*, 2005; *Stark et al.*, 2007; *Wingenter et al.*, 2005; *Yvon et al.*, 1996]. In some locations near the coast, nocturnal oxidation rates were sufficiently large to balance the DMS emission rate and effectively prevent vertical entrainment. In region 1, the calculated average reduction of DMS entrainment due to oxidation by NO_3 was $-0.7\ \mu mol\ m^{-2}\ d^{-1}$; in region 3, it was $-0.2\ \mu mol\ m^{-2}\ d^{-1}$. Consequently, the presence of NO_3 can affect the yield of sulfate aerosol from DMS emissions via two mechanisms: (1) reaction of DMS with NO_3 and subsequent peroxy radical reactions in the absence of NO changes the product distributions and may lead to the formation of more soluble species, and (2) the additional amount of oxidant present allows for depositional loss of condensable sulfur products derived from DMS oxidation within the marine boundary layer. Furthermore, since the removal of aerosols from the MBL is likely to be faster than in the layers above, the fraction of the DMS oxidized and not transported out of the MBL may influence sulfate aerosol production above the marine boundary layer. Last, our analysis is consistent with previous studies of photochemical DMS oxidation budgets in that photochemical oxidation appears faster than that due to OH alone, such that halogen species may play a role. There is no direct evidence, however, for nocturnal oxidation of DMS by halogens.

[30] **Acknowledgments.** The authors thank the crew and fellow scientists on board R/V *Brown* during NEAQS-ITCT 2004 and Roland von Glasow and Harald Stark for useful discussions in the preparation of this manuscript. Funding was provided in part by NOAA's Health of the Atmosphere program and in part by NOAA's Atmospheric Composition and Climate program.

References

Aldener, M., et al. (2006), Reactivity and loss mechanisms of NO_3 and N_2O_5 in a polluted marine environment: Results from in situ measurements during New England Air Quality Study 2002, *J. Geophys. Res.*, *111*, D23S73, doi:10.1029/2006JD007252.

Allan, B. J., et al. (2000), Observations of iodine monoxide in the remote marine boundary layer, *J. Geophys. Res.*, *105*, 14,363–14,369, doi:10.1029/1999JD901188.

Angevine, W. M., et al. (2006), Structure and formation of the highly stable marine boundary layer over the Gulf of Maine, *J. Geophys. Res.*, *111*, D23S22, doi:10.1029/2006JD007465.

Bandy, A., et al. (1996), Chemistry of dimethyl sulfide in the equatorial Pacific atmosphere, *Geophys. Res. Lett.*, *23*, 741–744, doi:10.1029/96GL00779.

Barnes, I., et al. (2006), Dimethyl sulfide and dimethyl sulfoxide and their oxidation in the atmosphere, *Chem. Rev.*, *106*, 940–975, doi:10.1021/cr020529+.

Bates, T. S., et al. (1998), Processes controlling the distribution of aerosol particles in the lower marine boundary layer during the First Aerosol Characterization Experiment (ACE 1), *J. Geophys. Res.*, *103*, 16,369–16,383.

Bates, T. S., et al. (2000), Aerosol physical properties and processes in the lower marine boundary layer: A comparison of shipboard sub-micron data from ACE-1 and ACE-2, *Tellus, Ser. B*, *52*, 258–272.

Brown, S. S., et al. (2004), Nighttime removal of NO_x in the summer marine boundary layer, *Geophys. Res. Lett.*, *31*, L07108, doi:10.1029/2004GL019412.

Brown, S. S., et al. (2005), Aircraft observations of daytime NO_3 and N_2O_5 and their implications for tropospheric chemistry, *J. Photochem. Photobiol. Chem.*, *176*, 270–278, doi:10.1016/j.jphotochem.2005.10.004.

Charlson, R. J., et al. (1987), Oceanic phytoplankton, atmospheric sulfur, cloud albedo and climate, *Nature*, *326*, 655–661, doi:10.1038/326655a0.

da Rosa, M. B., et al. (2003), Study of the heterogeneous reaction of O_3 with CH_3SCH_3 using the wetted-wall flowtube technique, *Atmos. Chem. Phys.*, *3*, 1665–1673.

De Bruyn, W. J., et al. (1998), Shipboard measurements of dimethyl sulfide and SO_2 southwest of Tasmania during the First Aerosol Characterization Experiment (ACE 1), *J. Geophys. Res.*, *103*, 16,703–16,711, doi:10.1029/98JD00971.

De Bruyn, W. J., et al. (2006), DMS and SO_2 measurements in the tropical marine boundary layer, *J. Atmos. Chem.*, *53*, 145–154, doi:10.1007/s10874-005-9000-z.

de Gouw, J. A., et al. (2005), Budget of organic carbon in a polluted atmosphere: Results from the New England Air Quality Study in 2002, *J. Geophys. Res.*, *110*, D16305, doi:10.1029/2004JD005623.

Faloona, I., et al. (2005), Observations of entrainment in eastern Pacific marine stratocumulus using three conserved scalars, *J. Atmos. Sci.*, *62*, 3268–3285, doi:10.1175/JAS3541.1.

Fehsenfeld, F. C., et al. (2006), International Consortium for Atmospheric Research on Transport and Transformation (ICARTT): North America to Europe—Overview of the 2004 summer field study, *J. Geophys. Res.*, *111*, D23S01, doi:10.1029/2006JD007829.

Gebel, M. E., et al. (2000), The uptake of SO_2 on synthetic sea salt and some of its components, *Geophys. Res. Lett.*, *27*, 887–890, doi:10.1029/1999GL011152.

Gershenzon, M., et al. (2001), Simultaneous uptake of DMS and ozone on water, *J. Phys. Chem. A*, *105*, 7031–7036, doi:10.1021/jp010696y.

Goldan, P. D., et al. (2004), Nonmethane hydrocarbon and oxy hydrocarbon measurements during the 2002 New England Air Quality Study, *J. Geophys. Res.*, *109*, D21309, doi:10.1029/2003JD004455.

Hynes, A. J., et al. (1986), Kinetics and mechanism of OH reactions with organic sulfides, *J. Phys. Chem.*, *90*, 4148–4156, doi:10.1021/j100408a062.

Jenkin, M. E., et al. (2003), Protocol for the development of the Master Chemical Mechanism, MCM v3(Part B): Tropospheric degradation of aromatic volatile organic compounds, *Atmos. Chem. Phys.*, *3*, 181–193.

Jensen, N. R., et al. (1992), Products and mechanisms of the gas-phase reactions of NO_3 with CH_3SCH_3, CD_3SCD_3, CH_3SH and CH_3SSCH_3, *J. Atmos. Chem.*, *14*, 95–108, doi:10.1007/BF00115226.

Jobson, B. T., et al. (1998), Spatial and temporal variability of nonmethane hydrocarbon mixing ratios and their relation to photochemical lifetime, *J. Geophys. Res.*, *103*, 13,557–13,567, doi:10.1029/97JD01715.

Langner, J., and H. Rodhe (1991), A global 3-dimensional model of the tropospheric sulfur cycle, *J. Atmos. Chem.*, *13*, 225–263, doi:10.1007/BF00058134.

Lucas, D. D., and R. G. Prinn (2002), Mechanistic studies of dimethylsulfide oxidation products using an observationally constrained model, *J. Geophys. Res.*, *107*(D14), 4201, doi:10.1029/2001JD000843.

Lucas, D. D., and R. G. Prinn (2003), Tropospheric distributions of sulfuric acid-water vapor aerosol nucleation rates from dimethylsulfide oxidation, *Geophys. Res. Lett.*, *30*(22), 2136, doi:10.1029/2003GL018370.

Lucas, D. D., and R. G. Prinn (2005a), Parametric sensitivity and uncertainty analysis of dimethylsulfide oxidation in the clear-sky remote marine boundary layer, *Atmos. Chem. Phys.*, *5*, 1505–1525.

Lucas, D. D., and R. G. Prinn (2005b), Sensitivities of gas-phase dimethylsulfide oxidation products to the assumed mechanisms in a chemical transport model, *J. Geophys. Res.*, *110*, D21312, doi:10.1029/2004JD005386.

Nightingale, P. D., et al. (2000), In situ evaluation of air-sea gas exchange parameterizations using novel conservative and volatile tracers, *Global Biogeochem. Cycles*, *14*, 373–387, doi:10.1029/1999GB900091.

Osthoff, H. D., et al. (2006), Observation of daytime N_2O_5 in the marine boundary layer during New England Air Quality Study–Intercontinental Transport and Chemical Transformation 2004, *J. Geophys. Res.*, *111*, D23S14, doi:10.1029/2006JD007593.

Pilling, M. J., and P. W. Seakins (1995), *Reaction Kinetics*, Oxford Univ. Press, Oxford, U. K.

Platt, U., et al. (2002), Free radicals and fast photochemistry during BERLIOZ, *J. Atmos. Chem.*, *42*, 359–394, doi:10.1023/A:1015707531660.

Pszenny, A. A. P., E. V. Fischer, R. S. Russo, B. C. Sive, and R. K. Varner (2007), Estimates of Cl atom concentrations and hydrocarbon kinetic reactivity in surface air at Appledore Island, Maine (USA), during International Consortium for Atmospheric Research on Transport and Transformation/Chemistry of Halogens at the Isles of Shoals, *J. Geophys. Res.*, *112*, D10S13, doi:10.1029/2006JD007725.

Roberts, J. M., et al. (1984), Measurements of aromatic hydrocarbon ratios and NOx concentrations in the rural troposphere—Observation of air-mass photochemical aging and NO_x removal, *Atmos. Environ.*, *18*, 2421–2432, doi:10.1016/0004-6981(84)90012-X.

Saiz-Lopez, A., et al. (2006), Measurements and modelling of I_2, IO, OIO, BrO and NO_3 in the mid-latitude marine boundary layer, *Atmos. Chem. Phys.*, *6*, 1513–1528.

Sander, S. P., et al. (2006), Chemical kinetics and photochemical data for use in atmospheric studies, *Eval. 15*, NASA/Jet Propul. Lab., Pasadena, Calif.

Saunders, S. M., et al. (2003), Protocol for the development of the Master Chemical Mechanism, MCM v3(Part A): Tropospheric degradation of non-aromatic volatile organic compounds, *Atmos. Chem. Phys.*, *3*, 161–180.

Singh, H. B. (1995), *Composition, Chemistry, and Climate of the Atmosphere*, 527 pp., Van Nostrand Reinhold, New York.

Sommariva, R., et al. (2008), Radicals in the marine boundary layer during NEAQS 2004: A model study of day-time and night-time sources and sinks, *Atmos. Chem. Phys. Discuss.*, *8*, 16,643–16,692.

Stark, H., et al. (2007), Influence of nitrate radical on the oxidation of dimethyl sulfide in a polluted marine environment, *J. Geophys. Res.*, *112*, D10S10, doi:10.1029/2006JD007669.

Suhre, K., et al. (1995), Biogenic sulfur emissions and aerosols over the tropical South Atlantic: 2. One-dimensional simulation of sulfur chemistry in the marine boundary layer, *J. Geophys. Res.*, *100*, 11,323–11,334, doi:10.1029/95JD00412.

Turnipseed, A. A., et al. (1996), Reaction of OH with dimethyl sulfide: 2. Products and mechanisms, *J. Phys. Chem.*, *100*, 14,703–14,713, doi:10.1021/jp960867c.

von Glasow, R., and P. J. Crutzen (2004), Model study of multiphase DMS oxidation with a focus on halogens, *Atmos. Chem. Phys.*, *4*, 589–608.

Warneke, C., et al. (2004), Comparison of daytime and nighttime oxidation of biogenic and anthropogenic VOCs along the New England coast in summer during New England Air Quality Study 2002, *J. Geophys. Res.*, *109*, D10309, doi:10.1029/2003JD004424.

Warneke, C., et al. (2007), Determination of urban volatile organic compound emission ratios and comparison with an emissions database, *J. Geophys. Res.*, *112*, D10S02, doi:10.1029/2006JD007589.

Wayne, R. P., et al. (1991), The nitrate radical—Physics, chemistry, and the atmosphere, *Atmos. Environ., Part A*, *25*, 1–203, doi:10.1016/0960-1686(91)90192-A.

Winer, A. M., et al. (1984), Gaseous nitrate radical—Possible nighttime atmospheric sink for biogenic organic compounds, *Science*, *224*, 156–159, doi:10.1126/science.224.4645.156.

Wingenter, O. W., et al. (2005), Atomic chlorine concentrations derived from ethane and hydroxyl measurements over the equatorial Pacific Ocean: Implication for dimethyl sulfide and bromine monoxide, *J. Geophys. Res.*, *110*, D20308, doi:10.1029/2005JD005875.

Yin, F. D., et al. (1990), Photooxidation of dimethyl sulfide and dimethyl disulfide: 1. Mechanism development, *J. Atmos. Chem.*, *11*, 309–364, doi:10.1007/BF00053780.

Yvon, S. A., et al. (1996), Atmospheric sulfur cycling in the tropical Pacific marine boundary layer (12°S, 135°W): A comparison of field data and model results: 1. Dimethylsulfide, *J. Geophys. Res.*, *101*, 6899–6909, doi:10.1029/95JD03356.

T. S. Bates and J. E. Johnson, Pacific Marine Environment Laboratory, NOAA, 7600 Sand Point Way, Seattle, WA 98115, USA.

T. Baynard, S. S. Brown, J. A. de Gouw, F. C. Fehsenfeld, P. Goldan, W. C. Kuster, B. M. Lerner, J. F. Meagher, A. Pettersson, A. R. Ravishankara, R. Sommariva, C. Warneke and E. J. Williams, Chemical Sciences Division, Earth System Research Laboratory, NOAA, 325 Broadway, Boulder, CO 80305, USA. (steven.s.brown@noaa.gov)

H. D. Osthoff, Department of Chemistry, University of Calgary, 2500 University Drive NW, Calgary, AB T2N 1N4, Canada.